

Development, Computational and Experimental Characterization of a Canard Aircraft Configuration

Pedro Miguel Micaelo Fernandes
pedro.micaelo.fernandes@tecnico.ulisboa.pt

Instituto Superior Técnico, Universidade de Lisboa, Portugal

November 2021

Abstract

The goal of this work is to structurally and aerodynamically design a new canard fixed-wing configuration with Vertical Take-Off and Landing (VTOL) capability Unmanned Aerial Vehicle (UAV) to be used by the Defense Research and Development Canada (DRDC) to detect submarines of the coast of Canada using a Magnetic Anomaly Detection (MAD) sensor. Initially, a surrogate based Multidisciplinary Design Optimization (MDO) process that was not yet finished is completed in order to reach a structurally and aerodynamically optimized solution. After the optimized solution was obtained, small design changes outside of the optimization process were analyzed to test their impacts on the aircraft performance. A design change to the canard was made due to stall speed requirements. One way Fluid Structure Interaction (FSI) simulations were performed to validate the structural integrity of the configuration. Changes were also made to the preliminary solution from the optimization process in this step. Finally, an extensive aerodynamic characterization of the aircraft was completed including a two way FSI at cruise condition. Next, the control surfaces were defined and estimates of the inertia of the aircraft were made. With these characteristics, a flight dynamics model was constructed using *Simulink* and the dynamic modes were studied to prove the stability of the aircraft. Finally, the projected wing was manufactured and static loading tests and Ground Vibration Tests (GVT) were performed in order to compare the manufactured specimen to a finite element model which can be used for future aeroelasticity analysis.

Keywords: Unmanned Aerial Vehicle, Multidisciplinary Design Optimization, Fluid-Structure Interaction, Flight Dynamics Model, Ground Vibration Tests, Static Load Tests.

1. Introduction

The motivation for this work is the design and development of a canard fixed-wing configuration with Vertical Take-Off and Landing (VTOL) capability Unmanned Aerial Vehicle (UAV) that is being pursued by the University of Victoria (UVic) Centre for Aerospace Research (CfAR) in collaboration with the Defense Research and Development Canada (DRDC), and it is meant to be used by the Canadian Air Force for Magnetic Anomaly Detection (MAD) operations of surveillance of the Canadian maritime borders. It will look for magnetic signals originating from submerged metallic vehicles, namely submarines.

This work is the continuation of the work done in two MSc theses. Bruno Luís did part of the conceptual and preliminary design so some decisions of the aircraft configuration were already established [1]. Then Tiago Jesus built a Multidisciplinary Design Optimization (MDO) tool in order to structurally and aerodynamically size the drone but whose optimization process was not yet converged [2]. The

major objective of this work is to complete the optimization and increase the detail of the design including aero-structural characterization, dynamic modeling and experimental validation.

2. Theoretical Background

2.1. Multidisciplinary Design Optimization

The first step in an optimization process is defining the problem. The objective function f is defined as a way to quantitatively measure how good a design is which allows the comparison between two different designs.

It is possible to state the optimization problem as:

$$\begin{aligned} &\text{Minimize} && f(\mathbf{x}) \\ &\text{w.r.t.} && \mathbf{x} \in \chi, \\ &\text{subject to} && h_i = 0, \quad i = 1, \dots, N_i \\ &&& g_j \geq 0, \quad j = 1, \dots, N_j. \end{aligned} \tag{1}$$

where \mathbf{x} is the set of design variables, χ is the design space, h is the vector of equality constraints

and g is the vector of inequality constraints which includes the bounds [3].

A surrogate model is a mathematical approximation that mimics the behavior of the system it is trying to substitute. It is generally much faster to compute but it is susceptible to large deviations from the real values. The surrogate model used in the MDO present in this project is a Kriging model [4].

Having the initial surrogate model, it is necessary to decide which new design points to evaluate in search of the global optimum. Four criteria were utilized to do this task in this MDO process: prediction based, expected improvement and Watson and Barnes Criteria WB2 and WB2S.

Instead of constraining the optimization of the objective function, it is possible to take the existing constraints into a probability of feasibility function that assesses the probability that the constraints are met. This can then be merged with the objective function in a new search function that will run unconstrained [4].

It is still necessary to choose the optimization algorithm to operate the search. Population methods are appropriate for the case of a surrogate optimization with an initial randomly obtained data base of points. The population method chosen for this MDO was a Genetic Algorithm (GA) [3].

2.2. Structural Analysis

For the structural analysis performed, Finite Element Analysis (FEA) are used with the help of *ANSYS Mechanical APDL* and *ANSYS Workbench* software. Since the materials used are Carbon Fiber Reinforced Polymers (CFRP), the Tsai-Wu failure criteria is used to check if there is structural failure [5].

The Finite Element Method (FEM) is a method used to approximately solve the differential equations that characterize the problem and that could be impossible to resolve from analytical methods.

The structure being tested is divided into subdomains called elements that form a mesh. The governing equations are approximated at each element by functions and algebraic equations that connect the solution values at a finite number of pre-selected points called element nodes. These equations are then combined through inter-element continuity of the solution and a balance of inter-element forces. The resulting simulation is a static analysis that is valid for all degrees of freedom [6].

Anisotropic material properties are direction dependent. This means that isotropic material failure criteria are not applicable and the strength and stress in all directions must be taken into account. Laminate composites are classified as orthotropic materials which is a subset of anisotropic materi-

als whose properties are different in three mutually orthogonal directions.

The Tsai-Wu criterion is a way to check for failure of CFRP. Because the Tsai-Wu criterion takes into account the interaction between different stress components it is usually better than other simpler criteria and is in agreement with experimental testing [5].

2.3. Aerodynamic Analysis

There are two types of aerodynamic analysis employed in this project.

A Low Fidelity (LF) calculation based on Prandtl's Lifting Line Theory (LLT) of the aerodynamic loads is used for the structural simulations during the optimization process. Prandtl's LLT is a simple solution for analyzing the aerodynamic behavior of unswept 3D wings with no dihedral and an $AR \geq 4$. Taking into account the twist and chord variation along the span, this theory is a good approximation when dealing with incompressible, inviscid and steady flow problems [7].

High Fidelity (HF) Computational Fluid Dynamics (CFD) analysis are used with the software *ANSYS CFX* for the aerodynamic characterization of the aircraft. *Ansys CFX* is a CFD software based on the Finite Volume Method (FVM). The governing equations in *Ansys CFX* are the unsteady Navier-Stokes Equations which describe the conservation of mass, momentum in the three directions and energy. The turbulence model used for this project was the Shear Stress Transport (SST) which is a two-equation eddy-viscosity model. It introduces two additional transport equations, one for the turbulent kinetic energy k and another for either the turbulent dissipation ϵ or the turbulent frequency ω . Each combination stems two different models, the $k - \epsilon$ or the $k - \omega$ respectively.

2.4. Fluid-Structure Interaction

The demand for an increase in accuracy in science and engineering simulations today more constantly requires the coupling of multiple physical fields. One of the most common but also challenging multi-disciplinary problems are Fluid-Structure Interactions (FSI), *i.e.*, interactions between one or more solid elastic structures with an internal or surrounding fluid flow.

The FSI simulations in this project will be made through *Ansys Workbench* by coupling the previously mentioned CFD capabilities of *Ansys CFX* with the structural analysis of *Ansys Mechanical*. A partitioned approach with a conforming mesh will be used [8, 9].

2.5. Flight Dynamics

Flight Dynamics is the study of the movement of an aircraft through the air and how the forces act-

ing on the vehicle influence its velocity and attitude through time. The dynamic equations of the rigid aircraft are obtained from the linearized Newton-Euler equations for linear and angular momentum.

A space state is used to evaluate the aircraft's dynamic modes. Each motion has multiple dynamic modes and each mode is characterized by its eigenvalue or poles. For an aircraft to be dynamically stable it has to be stable in both the longitudinal and lateral motions, which means that all the eigenvalues of the previously mentioned modes have to have a negative real part [10].

2.6. Modal Analysis

Modal analysis deals with the dynamic characteristics of mechanical structures and with the identification of their natural frequencies and mode shapes. Structures vibrate and deform in a specific mode shape when excited at their natural frequencies.

The identification of the mode shapes happens through the measurement of the Frequency Response Functions (FRFs) at multiple locations that, when combined, describe the frequency response of the entire structure which can be used to formulate a modal model for studying its dynamic behavior [11, 12].

2.7. Ground Vibration Tests

One of the experimental tests that aid in the realm of aeroservoelasticity is Ground Vibration Testing (GVT). These tests serve to experimentally measure the aircraft structural vibration modes which can be used to adjust FEM models for further analysis like calculating aeroelastic instability phenomena [13].

GVT works by measuring the acceleration response of the structure relative to the force excitation applied to the aircraft which will be recorded as FRFs.

3. Multidisciplinary Design Optimization

The optimization tool and process was built and defined by Tiago Jesus [2] but it had not yet converged as of the beginning of this work.

3.1. Mission Requirements

In order to formulate the optimization problem, define the objective function and set constraints, it is necessary to establish the requirements of the aircraft and the mission. The relevant information for this design process is the following:

1. Payload: the payload of this aircraft will be the MAD sensor and the electrical power supplies required for the correct functioning of the sensor. Its position must be such that the distances to engines and strong electrical currents do not affect the magnetic detection. This is

what led to the decision to use a canard configuration as the payload will be in the front of the aircraft as far away as possible from most of the electrical components which are in the back;

2. Speed and Wind: The aircraft must be capable of following a submarine that is traveling in the direction of the wind. For these reasons, the cruise speed V_{cruise} was set to 35 m/s. Considering V_{cruise} and the stronger wind gusts in the Arctic, the dash speed was set to 60 m/s;
3. MTOM: The Maximum Take-Off Mass (MTOM) was set to 25 kg, which allowed for an exemption from the requirement to obtain a Special Flight Operations Certificate (SFOC);
4. Maximum operational Load Factor: The maximum acceleration the aircraft was set to withstand is $3g$. This was decided during team meetings, as it is a typical value for general aircraft;
5. Stability: The static margin (K_n) was defined as being 10% of the mean aerodynamic chord and the vertical tail volume coefficient (C_{VT}) was settled at 0.02.

3.2. Objective Function

The ultimate objective of the optimization problem is to maximize range. Through the use of the weighted sum method, it is possible to evaluate the variation of range relative to a reference aircraft configuration. By approximating the range R from the Breguet equation as varying linearly with the Lift to Drag Ratio L/D and the structural mass m_s we get the following expression [14]:

$$\frac{\Delta R}{R_{ref}} = \frac{\Delta(L/D)}{(L/D)_{ref}} - \frac{\ln\left(1 + \frac{m_{s_{ref}}}{m_f}\right)}{\ln\left(\frac{m_i}{m_{f_{ref}}}\right)} \frac{\Delta m_s}{m_{s_{ref}}}, \quad (2)$$

where m_f is the final mass of the aircraft at the end of the mission segment and Δ represents the difference between the configuration being tested and the current best reference configuration. Because the goal is to maximize range but the objective function will be minimized, the symmetric of equation 2 is the function provided to the optimizer.

3.3. Design Variables and Parametrization

Each design point includes geometric, aerodynamic and structural variables. These are used to build aerodynamic and structural models to evaluate the L/D in cruise and m_s of the aircraft.

Table 1 lists all the design variables including the upper and lower bounds.

Table 1: Design variables with correspondent lower and upper bounds and respective units.

Variable	L.B.	U.B.
y_{scale} [-]	1	1.05
z_{scale} [-]	1	1.05
thk_{fuse} [m]	0.002	0.005
r_{tube} [m]	$0.2c_c t_c$	$0.9c_c t_c$
thk_{tube} [m]	$0.2r_{tube}$	r_{tube}
$pos_{f_{spar}}$ [m]	$0.1c(y)$	$0.25c(y)$
$thk_{tip_{spar}}$ [m]	8×10^{-4}	1.5×10^{-3}
$thk_{disc_{spar}}$ [m]	8×10^{-4}	3×10^{-3}
$thk_{root_{spar}}$ [m]	1×10^{-3}	5×10^{-3}
$thk_{tip_{skin}}$ [m]	6×10^{-4}	1.5×10^{-3}
$thk_{disc_{skin}}$ [m]	6×10^{-4}	2×10^{-3}
$thk_{root_{skin}}$ [m]	6×10^{-4}	3×10^{-3}
b_w [m]	2.3	4
c_{root_w} [m]	0.15	0.5
c_{disc_w} [m]	0.1	c_{root_w}
c_{tip_w} [m]	0.1	c_{disc_w}
$y_{c_{disc}}$ [m]	$0.3b_w/2$	$0.7b_w/2$
$\gamma_{w_{root}}$ [°]	-3	10
$\gamma_{w_{disc}}$ [°]	$\gamma_{w_{root}} - 3$	$\gamma_{w_{root}}$
$\gamma_{w_{tip}}$ [°]	$\gamma_{w_{disc}} - 3$	$\gamma_{w_{disc}}$
$y^{\gamma_{w_{disc}}}$ [m]	$0.3b_w/2$	$0.7b_w/2$
Λ_w [°]	0	30
t_w [-]	0.1	0.15
cbr_w [-]	0	0.07
b_{wgl} [m]	0.05	0.2
λ_{wgl} [-]	0.2	0.6
Λ_{wgl} [°]	0	30
t_{wgl} [-]	0.08	0.12
cbr_{wgl} [-]	0	0.02
b_c [m]	1	2
S_c [m ²]	$0.15S_w$	$0.25S_w$
l_c [m]	1.5	3.5
z_c [m]	pos_{bot}^1	pos_{top}^1
cbr_c [-]	0	0.07
c_{root_f} [m]	0.1	0.2
λ_f [-]	0.2	0.6
b_f [m]	0.2	0.4

¹ pos_{top} and pos_{bot} correspond to the most top and bottom positions on the fuselage spar with a safety margin for placing the canard.

3.4. MDA Procedure

There are two disciplines in the Multidisciplinary Design Analysis (MDA) of this work, structures and aerodynamics.

The analysis can be split into the following steps:

1. Generation of the structural geometry based on the inputs for the design variables;
2. LF estimation of the aerodynamic loading on the lifting surfaces (wing and canard) based on Prandtl's LLT;

3. Structural FEM analysis using the previously calculated aerodynamic loads to determine the structural mass and evaluate structural integrity;
4. If the structure is feasible than the Outer Mold Line (OML) for the HF aerodynamic simulations is created;
5. HF CFD analysis are performed to determine both trim and stability conditions and to gather performance results.

The structural model is created in *Ansys Mechanical APDL*. Besides the geometric dimensions it was also necessary to provide the material properties of each section. The structure is made of CFRP, either unidirectional (UD) carbon-epoxy or bidirectional woven carbon-epoxy.

The OML of the entire aircraft for the aerodynamic analysis is generated using *SOLIDWORKS*.

3.5. Optimization Results

Before the surrogate models were created, there were 8 fully evaluated configurations and the best one was considered the initial reference. It had the following properties:

- $m_{S_{ref}} = 9.731$ kg;
- $m_{f_{ref}} = 19.462$ kg;
- $L/D = 13.6$.

Tiago Jesus fully evaluated 33 different configurations for his thesis work. The design point with the best performance he achieved had the following properties:

- $m_{S_{ref}} = 4.209$ kg;
- $m_{f_{ref}} = 13.940$ kg;
- $L/D = 16.6$.

This means that the range of this configuration was 2.85 times greater than the original reference configuration.

However, the optimization had not yet fully converged. For this work, 39 more fully analyzed design points were studied for a total number of 72 iterations. Out of those 39, 12 were introduced by the author to help the exploration of the design space get configurations with better range.

Figure 1 plots the evolution of the ratio R/R_{ref_0} along the optimization, where R_{ref_0} is the range of the initial reference configuration.

From iteration 51 until 73 there was only one increase in range in iteration 61. This is the interval where the optimization process can be classified as converged, since more iterations are not able to bring better results.

From iteration 55 to iteration 73 the range ratio R/R_{ref_0} is about 3.45 which means that these configurations can go 3.45 times as far as the initial reference.

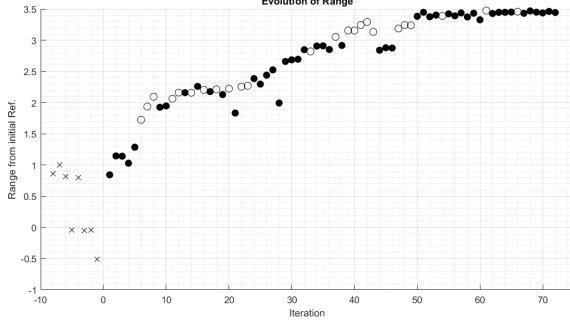


Figure 1: Evolution of the range ratio R/R_{ref0} along the optimization.

3.6. Final configuration

Two configurations were chosen out of the last 24 configurations that all had a similar range. Out of these, only one could go through with the analysis. Configuration number 68 was chosen as the final configuration.

The function outputs from this design point are:

- $m_s = 3.457$ kg;
- $m_f = 13.188$ kg;
- $L/D = 18.457$;
- $R/R_{ref0} = 3.468$.

In comparison with the initial reference configuration, the structural mass is 64.5 % lower and the lift to drag ratio is 35.7 % higher which combined gives a 3.468 times higher range. When comparing to the best configuration up until iteration 33, m_s still decreased 17.9 % and the L/D increased 11.2 % which means that the range increased in total 21.7 % which proves that there was still room for improvement at the beginning of this work.

Figure 2 illustrates the most relevant dimensions of the final aircraft configuration.

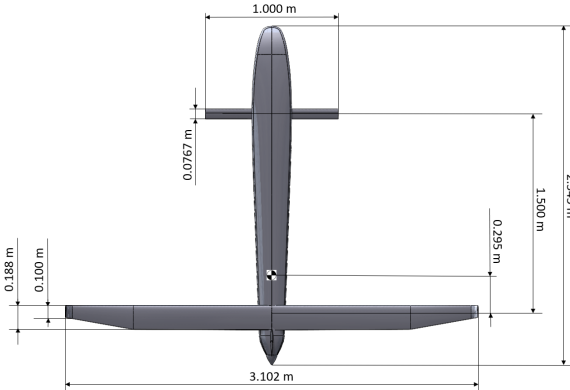


Figure 2: Geometric dimensions of configuration 68.

Figure 3 shows the Tsai-Wu failure index distribution along the structural components. The Wing skin is one of the components that carries the

biggest loads and if the laminate had fewer layers it would not be able to withstand the aerodynamic forces.

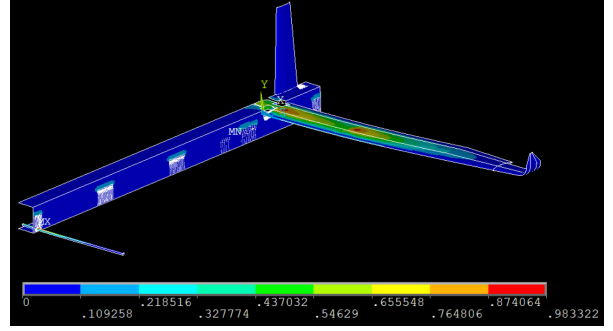


Figure 3: Tsai-Wu failure index values on the entire aircraft structure.

4. Aircraft Characterization

4.1. Stall Speed Determination

The next step in validating the design was determining the stall speed V_{stall} . The requirements for this parameter are related to the testing of the aircraft. For it to be tested near CfAR's headquarters, the cruise speed can not exceed 28 m/s as it would be too difficult to maneuver it safely within the testing field. Considering a cruise speed 1.3 times higher than the stall speed, which is standard practice in aviation, V_{stall} should be at the maximum 21.5 m/s.

To calculate the stall speed, 12 CFD simulations were performed with varying angles of attack between -5° and 17° to get the C_L and C_m values in regards to the angle of attack for the wing, canard, and fuselage separately.

To calculate the stall speed one must solve the system of equations 3 to determine the unknown variables V_{stall} and α_{stall} where the m and b coefficients are obtained from linear trendlines applied to the C_L and C_m vs α results.

$$\begin{aligned} & \begin{cases} M = 0 \\ L_c + L_{w+fus} = m_i g \end{cases} \Leftrightarrow \\ & \Leftrightarrow \begin{cases} C_{m_{cmax}} + C_{m_{w+fus}} = 0 \\ \frac{1}{2} \rho S_w V_{stall}^2 (C_{L_{cmax}} + C_{L_{w+fus}}) = m_i g \end{cases} \Leftrightarrow \\ & \Leftrightarrow \begin{cases} C_{m_{cmax}} + m_2 \alpha_{stall} + b_2 = 0 \\ \frac{1}{2} \rho S_w V_{stall}^2 (C_{L_{cmax}} + m_1 \alpha_{stall} + b_1) = m_i g \end{cases} \end{aligned} \quad (3)$$

Solving the system of equations for the aircraft at hand one gets $V_{stall} = 26.205$ m/s, $\alpha_{stall} = 6.464^\circ$ and $i_c = 6.536^\circ$.

This stall speed is not low enough because the aircraft would have to be flown dangerously close to the stall speed when testing. Thus, two more

aircraft designs where the canard area was changed were analyzed. The first aircraft, which will be addressed as configuration 68-20, has a 20% bigger canard area and was used to test what would be the difference in the stall speed of a small change in the canard area. Configuration 68-109 or the second one has a 109 % bigger canard area and was used to see what would be the difference of a more significant change in canard area.

By applying the same process that was done to configuration 68, the cruise and stall conditions were evaluated for these two new configurations. With these results, table 2 was built.

Table 2: Comparison of the three configurations and their stall properties.

	68	68-20	68-109
L/D_{cruise} [-]	18.457	18.233	17.774
$i_{c_{trim}}$ [°]	2.926	2.199	0.602
α_{trim} [°]	1.968	1.857	1.364
V_{stall} [m/s]	26.205	24.974	22.608
V_{cruise}/V_{stall} [-]	1.336	1.401	1.548
α_{stall} [°]	6.464	7.317	8.701
m_c [g]	178.6	214.5	374
ΔR_{mass}^1 [%]	0	-0.80	-4.36
ΔR_{total}^2 [%]	0	-2.01	-7.90

¹ This difference in range due to the extra structural mass was calculated by assuming the original configuration had 5 kg of fuel. ² The total range difference is the sum of the differences caused by the decrease in L/D and the extra structural mass.

After this study was performed, it was decided to progress the rest of the analysis of this project with the 68-109 configuration. Even though the stall speed does not meet the 21.5 m/s requirement, it was decided that 22.6 m/s was enough to test the aircraft at 28 m/s, which gives a testing speed over stall speed ratio of 1.24. If in the future the extra range of the original configuration proves to be necessary, then the canard can be reverted to its original state which was considered an easy implementation without big impacts on the design of the rest of the aircraft.

Furthermore, a *MATLAB* program was built to estimate the stall speed based on the canard to wing area ratio and the wing area. From that program, the graph in figure 4 was created.

4.2. Winglet modification

Before the final OML of the aircraft was established, one last adjustment was made to the winglet design. The way the winglet was defined during the optimization process made it so that the final shape had sharp corners and edges and an overall not smooth transition from the tip of the wing to the tip of the

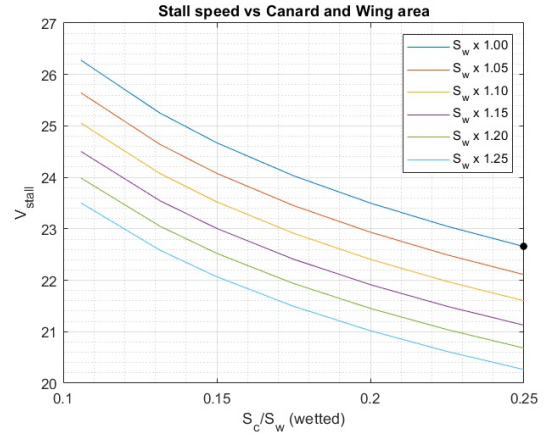


Figure 4: Stall speed calculation based on wing and canard area. Black dot signals the chosen configuration going forwards (68-109).

winglet. For these reasons, it was decided that the winglet design could be refined. It was possible to increase the L/D from the original 17.774 for the 68-109 configuration to 17.815, which represents a 0.23 % increase. This increase is somewhat negligible but at least it shows that the change likely does not negatively impact the performance.

4.3. Structural Validation

The structure of the aircraft suffered several changes in order to get a lighter structure and to increase the available space inside the fuselage.

The first is related to the fuselage. The decision was to transform the OML of the fuselage into a structure that supports its own loads. The spars were far from breaking in the ultimate load condition, which means that there is extra material that can be removed in order to reduce the structural mass. The implementation of a core material allows for a lighter structure while keeping the thickness and, in turn, the stiffness high. The core material used is a homogeneous PVC foam. The laminate will then be a sandwich composite composed of one layer of woven carbon fiber at a 45° angle with the aircraft longitudinal axis on each side of one layer of core material.

The second structural change is related to the canard. Similar to the fuselage, there is still the need to make the outside skin even with the canard tube. For this reason, it was decided it was best to make the skin of the canard the main load-carrying structure.

With this in mind, a Computer-Aided Design (CAD) surface model was made in *SOLIDWORKS*. This model was imported to *Ansys Workbench* and the composite definition of each surface was done using the *Ansys Composite PrePost* module (ACP).

For a better analysis of the structure, instead of using the aerodynamic loads calculated from the LF Prandtl's LLT, a one-way FSI employing CFD analysis was used. The loading condition is still the 4.5g pull-up maneuver. The resulting pressure on the surfaces of the aircraft is then imported to *Ansys Mechanical* and applied to the structure surfaces.

The structural analysis is then run with large deflections on. Large deflections on makes the load be applied in increments and after each substep, the stiffness matrix K of the structure is recalculated to take into account the deformed state.

After running the simulation it was found that the wing structure from the optimization process is not capable of withstanding the aerodynamic loads for the ultimate conditions. Figure 5 shows a close-up of the Tsai-Wu failure index in the wing root section.

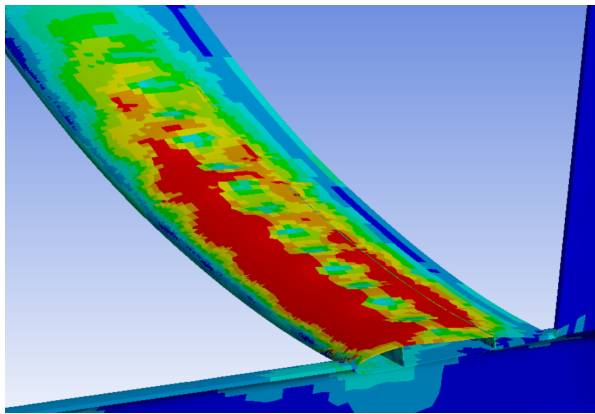


Figure 5: Close-up of Tsai-Wu failure index on wing.

The solution to this situation is a redesign of the composite layup. The top surface will be different from the bottom surface since CFRP is weaker in compression than in tension. The top skin will have the same core as the fuselage between the two spars to eliminate buckling. The woven layers will be placed at 90° instead of 45° because it was found these are better at carrying the loads and the composite will always be symmetric.

With this new layup sequence, the structural simulation was reevaluated. The Tsai-Wu failure index for this scenario is available in figure 6.

The maximum Tsai-Wu failure index in the new composite lay-up is 0.703 near the root section which does not exceed the critical value of 1.

The total estimated mass of the structural components is 3.316 kg. This means that the mass decreased from the original configuration from the optimization process.

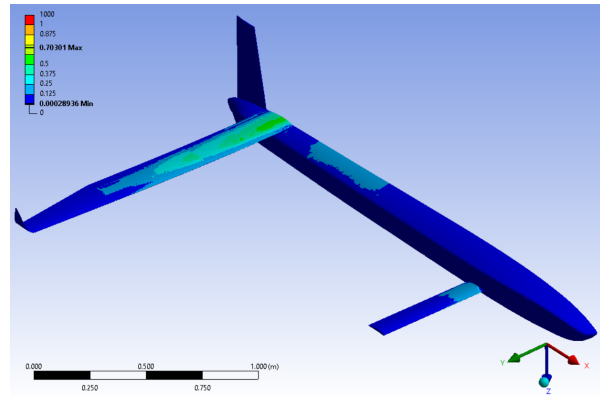


Figure 6: Tsai-Wu failure index on aircraft.

4.4. Aircraft Performance

With the final aerodynamic design done and the final composite structures defined, the aircraft performance can be further characterized.

The cruise performance will be accessed by a two-way FSI simulation. This simulation will determine the aerodynamic performance of the aircraft taking into account the deformation caused by the aerodynamic loads.

After running the analysis, it was discovered that the L/D in cruise condition is 17.800 which is a 0.15 % better result than with just the CFD analysis. This shows that the fluid forces deform the structure in a way that should not decrease the aerodynamic coefficients.

By analyzing the pressure distribution around the aircraft and on the symmetry plane as seen in figure 7 it is possible to see that the canard has a higher pressure differential than the wing.

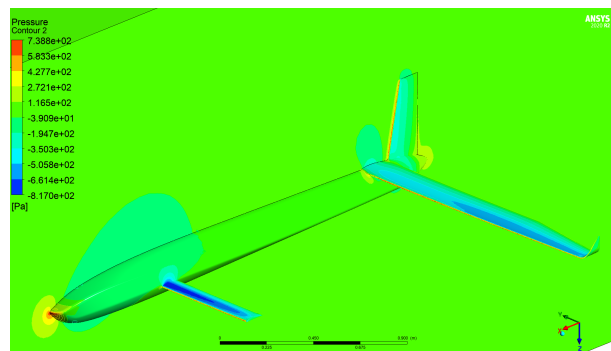


Figure 7: Pressure distribution on the aircraft's surfaces and symmetry plane.

To characterize the aircraft at speeds besides the cruise condition, one can use the simulations to calculate the stall speed to find the trim condition at all speeds between the stall speed and the dash speed.

Through the use of a *MATLAB* program, the

trim condition was calculated for speeds between 23 m/s and 60 m/s. From it, the L/D vs airspeed, the trim angles vs airspeed, and the power and thrust necessary from the propulsion system were calculated.

4.5. Control Surfaces Design

The design of the control surfaces was based on empirical data from [15].

The following values were chosen for the ailerons of this aircraft:

- $\frac{b_{a_i}}{b_w} = 0.72$;
- $\frac{b_a}{b_w} = 0.26$;
- $\frac{c_a}{c_w} = 0.25$;
- $\frac{S_a}{S_w} = 0.0558$;

The following values were chosen for the geometry of the rudder:

- $\frac{b_{r_i}}{b_f} = 0.05$;
- $\frac{b_r}{b_f} = 0.9$;
- $\frac{c_r}{c_f} = 0.25$;
- $\frac{S_r}{S_f} = 0.225$;

4.6. Flight Dynamics Model

A Flight Dynamics Model of the aircraft allows for the simulation of its behavior in different flying scenarios. The first step in creating the FDM is getting the derivatives that characterize the motion of the aircraft according to the control inputs and the current aircraft state. Using the simulations from the stall speed calculations, new simulations to get the control surfaces and the side slip angle β coefficients and also equations to calculate the angular velocity components p , q and r coefficients, all the coefficients that characterize the aircraft were determined.

Another important piece of information that remains to be calculated is the inertia of the aircraft. Since most of the systems that will go on the aircraft have yet to be defined, their weight and dimensions are unknown. For this reason, some assumptions had to be made to estimate the inertia.

The resulting inertia matrix of the aircraft with the components inside is:

$$I = \begin{bmatrix} 0.97255 & 0 & -1.13462 \\ 0 & 16.2584 & 0 \\ -1.13462 & 0 & 17.1078 \end{bmatrix}.$$

With the inertia and the aerodynamic coefficients defined, a *Simulink* model was created. Running this model starts with a *MATLAB* script that defines all the aircraft properties as well as the initial state, which includes the initial position, velocity, Euler angles, and angular velocity. The model then simulates the aircraft behavior until a certain end

time based on the control inputs δ_{i_c} (canard incidence angle), δ_A (aileron deflection angle), δ_R (rudder deflection angle) and δ_T (thrust percentage) and the current state of the aircraft.

4.7. Stability

To determine the aircraft stability characteristics at the trim condition for different velocities, another *MATLAB* program was constructed. This program takes the trim conditions previously calculated and solves the dynamic equations to calculate the eigenvalues for both longitudinal and lateral modes.

All modes were found to be stable at all operational speeds except the spiral mode at 23 m/s.

5. Experimental Testing

In order to validate the Finite Element (FE) model of the wing, static load tests as well as GVT were performed on a manufactured sample.

5.1. Manufacturing

The composite wing was manufactured using the open mold hand lay-up process. The first step was designing the molds using *SOLIDWORKS* which have the negative OML of the wing.

The wing skin was divided along the leading and trailing edges, resulting in a separation between the top and bottom surfaces. Each surface was divided in four different molds, two on each side, one for the planar wing surface and another for the winglet. Each wing skin was then manufactured.

The spars were manufactured on a flat table, but the lay-up process was the same as for the skins. Because of the angle change at the chord discontinuity, each spar was divided into three pieces, one middle piece and two tip pieces.

The spars and rib were then glued with epoxy resin to the top surface of the wing in their respective locations. After the resin cured, the internal elements were sanded until the lower surface fitted correctly on the upper surface. The next step was gluing the lower surface to the rest of the structure. Epoxy resin was applied to the leading and trailing edges and to the upper edges of the spars to ensure the connection between both surfaces.

After the epoxy resin cured, the last step is to cut the composite flashing and the aileron cut-outs and fill any holes in the leading edge that may have appeared. Figure 8 shows a picture of the manufactured wing.

The manufactured wing had a final mass of 1.716 kg, 32.5 % heavier than the expected mass of the FE model of the wing without ailerons of 1.295 kg.

5.2. Ground Vibration Testing

The first performed test on the wing was the GVT. The wing was supported by a cable to simulate a free-free boundary condition as close as possible. Four uniaxial sensors were placed on the wing



Figure 8: Manufactured wing.

and one of the winglets to collect accelerations and through a previously developed *LabView* interface, the FRFs were computed by making use of the data also collected from the impact hammer. Both out-of-plane and in-plane information was collected, adding to a total of 54 locations on the wing where either the impact hammer hit or the sensors were placed and a total of 81 Degrees of Freedom (DOFs).

The frequency range of interest for this wing was considered to be from 0 Hz until 200 Hz. For this reason, the impact hammer was equipped with a soft tip. Three successful hits per point were necessary in order to collect the FRFs.

The collected data was then processed with *MEScope* where a model of the wing defined by the impact points was built in order to post-process the data.

The computational and experimental results were used to build table 3. It shows the modes whose frequencies are under 200 Hz, the disparity between both acquired frequencies as well as the damping from the GVT. Some abbreviations were used to describe the mode shape: *anti.* means anti-symmetrical, *sym.* means symmetrical, *OP* means out-of-plane and *IP* means in-plane.

Furthermore, two winglet mode shapes were also detected in both the FE model and the GVT. Three Rigid-Body Motions (RBM) frequencies were detected in the experimental results as well.

5.3. Wing Static Loading

For the static loading tests, the wing was glued to an aluminum plate which was then bolted against a metal support that was secured to the ceiling to secure the wing in a fixed position.

The wing lift was simulated through the use of iron weights and sandbags. Since the lift points upwards and the weight of these masses point downwards, the wing was fixed upside down.

To better analyze the deformation of the wing under loading, a photogrammetry software called *Regard3D* was used. The technique this program uses consists of extracting 3D information from photographs of an object to reconstruct it into a 3D

model.

To get the shape in the loaded and unloaded conditions, multiple photographs had to be taken. These were then triangulated to get a point cloud which was then imported into another software called *MeshLab* for post-processing.

The wing root bending moment in cruise is estimated to be 65.6 N.m from the *Ansys CFX* analysis. To test this loading condition, it was decided to use a single mass of 6.43 kg at the chord discontinuity 1.04 m away from the root chord.

A simulation in *Ansys Mechanical* was performed to evaluate the deformation of the FE model of the wing with this force applied and compare it with the experimental results.

The point clouds from the photogrammetry software were used to extract the 3D position of several points in the Leading Edge (LE) and Trailing Edge (TE) of both the deformed and undeformed states. By also extracting the position of the leading and trailing edge from the results from *Ansys*, figure 9 was created in *MATLAB* which shows the deformed and undeformed shapes from both methods.

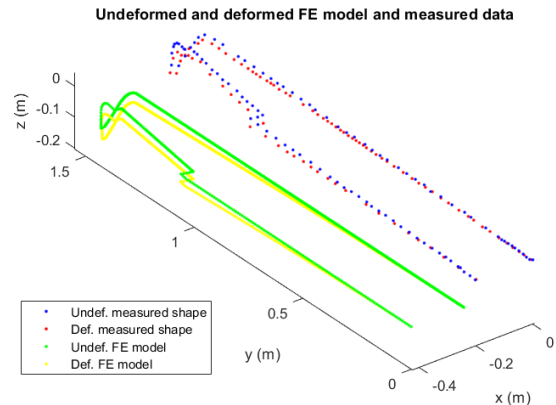


Figure 9: 3D plot of the deformed and undeformed LE and TE from both experimental and computational results.

It is possible to use photogrammetry to determine the deformation of the wing and to get a 3D model. However, the errors associated with the determination of each point make the fidelity of the displacement calculations low. Since this loading case had a small maximum displacement, this uncertainty results in a high relative error. If the loading conditions tested are higher, the relative error should be smaller.

After the cruise loading condition was tested, the operational load limit case scenario of $3g$ and the ultimate loading condition of $4.5g$ for which the wing was designed were tested.

The wing did not break, no cracking sounds were heard and no buckling was visible. This validated

Table 3: Sensor locations and Degrees of Freedom.

Mode #	Mode shape	f_{FEA} [Hz]	f_{GVT} [Hz]	Δf [%]	ζ [%]
1	1st OP sym. bending	23.1	25.8	+11.7	1.2
2	1st OP anti. bending	46.3	43.8	-5.4	0.3
3	1st torsion	67.4	81.1	+20.3	0.4
4	2nd OP sym. bending	77.4	74.5	-3.7	1.1
5	2nd OP anti. bending	108.6	107.0	-1.5	0.8
6	2nd torsion	121.1	132.0	+9.0	1.1
7	3rd OP sym. bending	161.9	158.0	-2.4	0.2
8	1st IP sym. bending	172.5	158.0	-8.4	0.6
9	3rd torsion	178.2	197.0	+10.5	1.0

the wing for the ultimate load limit of 4.5g.

6. Conclusions

Convergence was achieved in the optimization process. The structural and aerodynamic design of the aircraft was successfully completed. The control surfaces were defined and the aerodynamic coefficients determined. A Flight Dynamics Model was created and the stability of the aircraft was proven. The projected wing was built, tested and compared to the FE model.

Due to the high aspect ratio of the wing, aeroelastic phenomena like flutter and divergence can become a problem so they should be studied. The experimental results from the GVT and the static load tests can be used to update a simplified beam model of the wing whose characteristics can then be used to determine the flutter and divergence speed and guarantee that these are outside the operational envelope of the aircraft.

Acknowledgments

The author would like to thank his supervisors, Professor Afzal Suleman and Dr. José Lobo do Vale, as well as his friends and family for all the support given throughout this work.

References

- [1] B. M. W. Luís. Design and development of a magnetic anomaly detection unmanned aerial vehicle. Master's thesis, Instituto Superior Técnico, 2019.
- [2] T. A. S. Jesus. Surrogate-based multidisciplinary design optimization of a canard configuration vtol uav. Master's thesis, Instituto Superior Técnico, 2020.
- [3] Mykel J. Kochenderfer and Tim A. Wheeler. *Algorithms for Optimization*. The MIT Press, 2019.
- [4] Alexander I. J. Forrester, Andrés Sóbester, and Andy J. Keane. *Engineering Design via Surrogate Modelling*. Wiley, jul 2008.
- [5] Matthew L. Camilleri. *Structural analysis*. 2010.
- [6] D. J N Reddy. *An Introduction to the Finite Element Method*. McGraw-Hill Education, 2005.
- [7] Snorri Gudmundsson. Chapter 9 - the anatomy of the wing. In Snorri Gudmundsson, editor, *General Aviation Aircraft Design*, pages 299–399. Butterworth-Heinemann, Boston, 2014.
- [8] Gene Hou, Jin Wang, and Anita Layton. Numerical Methods for Fluid-Structure Interaction — A Review. *Communications in Computational Physics*, 12(2):337–377, aug 2012.
- [9] Bungartz Hans-Joachim and Michael Schäfer. *Fluid-Structure Interaction*, volume 53 of *Lecture Notes in Computational Science and Engineering*. Springer Berlin Heidelberg, Berlin, Heidelberg, 2006.
- [10] J. Oliveira. *Flight Stability - Class Notes*. 2019.
- [11] G. Kerschen, M. Peeters, J. C. Golinval, and C. Stéphan. Nonlinear modal analysis of a full-scale aircraft. *Journal of Aircraft*, 50(5):1409–1419, 2013.
- [12] M. Peeters, G. Kerschen, and J. C. Golinval. Dynamic testing of nonlinear vibrating structures using nonlinear normal modes. *Journal of Sound and Vibration*, 330(3):486–509, 2011.
- [13] Jan R. Wright and Jonathan E. Cooper. *Introduction to Aircraft Aeroelasticity and Loads*. John Wiley and Sons Ltd, Chichester, UK, dec 2014.
- [14] Tiago Jesus, Martin Sohst, José Lobo do Vale, and Afzal Suleman. Surrogate based MDO of a canard configuration aircraft. *Structural and Multidisciplinary Optimization*, sep 2021.
- [15] M. Sadraey. *Aircraft Design: A Systems Engineering Approach*. John Wiley and Sons Ltd, 2012.